# Visualizing atomic sizes and molecular shapes with the classical turning surface of the Kohn–Sham potential

Egor Ospadov[a], Jianmin Tao[b], Viktor N. Staroverov[a], and John P. Perdew[b,c,1]

[a]Department of Chemistry, The University of Western Ontario, London, ON N6A 5B7, Canada; [b]Department of Physics, Temple University, Philadelphia, PA 19122; and [c]Department of Chemistry, Temple University, Philadelphia, PA 19122

Contributed by John P. Perdew, September 28, 2018 (sent for review August 23, 2018; reviewed by Ernest R. Davidson and Mel Levy)

**The Kohn–Sham potential $v_{\rm eff}(\mathbf{r})$ is the effective multiplicative operator in a noninteracting Schrödinger equation that reproduces the ground-state density of a real (interacting) system. The sizes and shapes of atoms, molecules, and solids can be defined in terms of Kohn–Sham potentials in a nonarbitrary way that accords with chemical intuition and can be implemented efficiently, permitting a natural pictorial representation for chemistry and condensed-matter physics. Let $\epsilon_{\rm max}$ be the maximum occupied orbital energy of the noninteracting electrons. Then the equation $v_{\rm eff}(\mathbf{r}) = \epsilon_{\rm max}$ defines the surface at which classical electrons with energy $\epsilon \leq \epsilon_{\rm max}$ would be turned back and thus determines the surface of any electronic object. Atomic and ionic radii defined in this manner agree well with empirical estimates, show regular chemical trends, and allow one to identify the type of chemical bonding between two given atoms by comparing the actual internuclear distance to the sum of atomic radii. The molecular surfaces can be fused (for a covalent bond), seamed (ionic bond), necked (hydrogen bond), or divided (van der Waals bond). This contribution extends the pioneering work of Z.-Z. Yang et al. [Yang ZZ, Davidson ER (1997) *Int J Quantum Chem* 62:47–53; Zhao DX, et al. (2018) *Mol Phys* 116:969–977] by our consideration of the Kohn–Sham potential, protomolecules, doubly negative atomic ions, a bond-type parameter, seamed and necked molecular surfaces, and a more extensive table of atomic and ionic radii that are fully consistent with expected periodic trends.**

atomic radius | molecular surface | Kohn–Sham potential | chemical bonding | classical turning point

Our human minds are adapted to a three-dimensional classical world, identifying and visualizing objects by the sizes and shapes of their surfaces. This intuition serves us well even on the atomic scale of chemistry and condensed-matter physics: Atoms and atomic ions are essentially spheres of varying size that can bind together in several ways (1). In a covalent bond, atoms fuse together, losing much of their identity as they create a molecule or solid with a fused surface. In an ionic bond, positive and negative atomic ions retain more of their identity, binding together by long-ranged electrostatic forces. In a van der Waals bond, neutral atoms or molecules retain nearly all of their identity. A hydrogen bond is a mix of those three bond types (2).

How can we define, visualize, and represent the sizes and shapes of atoms, molecules, and solid surfaces (including any internal surfaces)? There have been many ingenious and useful constructions of the radii of atoms and atomic ions based upon the observed nuclear geometries of their bonded structures (for instance, refs. 3–8). But the underlying theory, quantum mechanics, does not seem to predict a sharp surface. Instead it predicts an electron density that is distributed nonuniformly over all of three-dimensional space, decaying exponentially at positions far enough away from an atom, ion, or molecule. One might define the surface as a particular isodensity contour (usually 0.001 $e/a_0^3$). Radii of atoms and singly positive ions determined in this manner for elements 1–96 were given by Rahm et al. (9). The drawback of this definition is that the choice of a cutoff density is somewhat arbitrary (10). Alternative definitions rely on surfaces of maximum radial electron density (8) (which do not generalize to nonspherical objects like molecules), isosurfaces of the electrostatic potential (11), fraction of the total electron density (12), and other ideas.

In classical physics, noninteracting electrons of maximum energy $\epsilon_{\rm max}$ bound by an effective potential $v_{\rm eff}(\mathbf{r})$ are confined inside the classical turning surface defined as the set of all points $\mathbf{r}$ that satisfy the condition

$$v_{\rm eff}(\mathbf{r}) = \epsilon_{\rm max}. \qquad [1]$$

Classical electrons are turned back when they strike this surface, although quantum-mechanical ones can tunnel out. In a series of pioneering papers, Yang and coworkers (13–21) explored atomic and molecular shapes defined as classical turning surfaces of the "potential acting on an electron in a molecule" (PAEM),

$$v_{\rm eff}^{\rm PAEM}(\mathbf{r}) = v_{\rm ESP}(\mathbf{r}) + v_{\rm XC}^{\rm hole}(\mathbf{r}), \qquad [2]$$

at $\epsilon_{\rm max} = -I$, where $I$ is the first vertical ionization energy of the system. In Eq. **2**, $v_{\rm ESP}(\mathbf{r})$ is the molecular electrostatic potential (ESP) and $v_{\rm XC}^{\rm hole}(\mathbf{r})$ is the potential of the exchange-correlation hole charge (22) derived from an interacting wavefunction. For a Hartree–Fock wavefunction, $v_{\rm XC}^{\rm hole}(\mathbf{r})$ is called the Slater potential (23).

## Significance

**Can quantum mechanics predict a well-defined and chemically intuitive size and shape for an atom or a molecule? We show that the bounding surface of a chemical species can be naturally defined as the classical turning surface of the Kohn–Sham potential—an effective potential that, acting on noninteracting electrons, yields the ground-state density of the real system. The atomic and ionic radii defined in this manner display all expected periodic trends, while the ratio of a bond length to the sum of atomic or ionic radii identifies the type of the bond (covalent, ionic, hydrogen, or van der Waals). The proposed approach permits a visual representation of chemical species that is intuitive and quantum-mechanically rigorous at the same time.**

Author contributions: E.O., J.T., V.N.S., and J.P.P. designed research; E.O., V.N.S., and J.P.P. performed research; E.O., V.N.S., and J.P.P. analyzed data; and V.N.S. and J.P.P. wrote the paper.

Reviewers: E.R.D., University of Washington; and M.L., Tulane University.

The authors declare no conflict of interest.



[1]To whom correspondence should be addressed. Email: perdew@temple.edu.

This article contains supporting information online at www.pnas.org/lookup/suppl/doi:10.1073/pnas.1814300115/-/DCSupplemental.

Published online November 21, 2018.



www.pnas.org/cgi/doi/10.1073/pnas.1814300115

Despite being conceptually fruitful, the definition of molecular surfaces in terms of PAEMs has a few weaknesses. First, the PAEM is not a functional derivative of any density functional (24, 25) and thus not a true effective potential. Second, the value of $\epsilon_{max} = -I$ has to be determined separately from the PAEM (for instance, taken from experiment). Third, the PAEM misses important structural features (26–29) and is too negative [because $v_{XC}^{hole}(\mathbf{r})$ is twice an ab initio exchange-correlation energy per electron]. As a consequence, atomic radii and molecular surfaces derived from PAEMs do not always follow the established chemical trends (21).

Now in the Kohn–Sham density-functional theory (30, 31), there is an exact effective potential $v_{eff}^{KS}(\mathbf{r})$ that, acting on fictitious noninteracting electrons, produces the same ground-state electron density as that of the real (interacting) electrons. Although not guaranteed to exist in every case (32, 33), $v_{eff}^{KS}(\mathbf{r})$ does exist for many systems of chemical interest, and useful approximations to it are always possible. The Kohn–Sham effective potential may be written as

$$v_{eff}^{KS}(\mathbf{r}) = v_{ESP}(\mathbf{r}) + v_{XC}^{KS}(\mathbf{r}), \quad [3]$$

where $v_{XC}^{KS}(\mathbf{r})$ is the Kohn–Sham exchange-correlation potential. The latter is related to $v_{XC}^{hole}(\mathbf{r})$ by

$$v_{XC}^{KS}(\mathbf{r}) = v_{XC}^{hole}(\mathbf{r}) + v_{resp}(\mathbf{r}) + v_{c,kin}(\mathbf{r}), \quad [4]$$

where $v_{resp}(\mathbf{r})$ and $v_{c,kin}(\mathbf{r})$ are, respectively, the response and kinetic correlation potentials, expressible in terms of the interacting wavefunction and the Kohn–Sham orbitals and orbital energies of the system (34–36). It is these two terms that make $v_{eff}^{KS}(\mathbf{r})$ qualitatively different from the PAEM. The value of $\epsilon_{max}$ is naturally determined by $v_{eff}^{KS}(\mathbf{r})$ as the energy of the Kohn–Sham highest occupied molecular orbital (HOMO) (26).

Here we propose to define atomic sizes and molecular shapes in terms of the classical turning surface of the exact Kohn–Sham effective potential, that is, by Eq. **1** with $\epsilon_{max} = \epsilon_{HOMO}^{KS}$. We show that the classical turning surface of the Kohn–Sham potential may be the most natural definition of molecular surface that quantum mechanics and density-functional theory can offer. We also demonstrate that atomic and ionic radii extracted from $v_{eff}^{KS}(\mathbf{r})$ are in full accord with chemical intuition and expected periodic trends. While the classical turning surface scales properly with system size, we show that simpler alternatives based on the electron density often do not.

## Methodology

The proposed definition of molecular surfaces requires construction of accurate Kohn–Sham effective potentials for atoms and molecules. Standard density-functional approximations are generally insufficient for this purpose because they tend to produce unrealistic exchange-correlation potentials (37).

Accurate Kohn–Sham potentials of many-electron systems have been traditionally obtained by fitting $v_{eff}^{KS}(\mathbf{r})$ to a given ab initio density (for instance, ref. 38 and references therein) or by solving the optimized effective potential (OEP) equation (39). Both of these approaches amount to solving an ill-posed inversion problem and are not well suited for routine applications on account of numerical instabilities and basis-set artifacts involved (40). The recently developed method for generating Kohn–Sham potentials from electronic wavefunctions (41–43) has made it possible to obtain high-quality Kohn–Sham potentials in a run-of-the-mill manner. Here we use the definitive version of this method, the modified Ryabinkin–Kohut–Staroverov (mRKS) procedure of ref. 43, which we implemented locally in the GAUSSIAN program (44).

The mRKS method takes an ab initio wavefunction of the system as input and produces the corresponding Kohn–Sham effective potential and its orbitals and orbital energies as output. In particular, when the mRKS procedure is applied to a Hartree–Fock wavefunction, it gives a Kohn–Sham-like multiplicative effective potential that, acting on noninteracting electrons, recovers the corresponding Hartree–Fock ground-state electron density with a small basis-set error vanishing in the basis-set limit. To ensure that $v_{eff}^{KS}(\mathbf{r})$ approaches the correct $r \to \infty$ limit, the mRKS procedure shifts the potential by a constant fixed by the condition

$$\epsilon_{HOMO}^{KS} = -I_{EKT}, \quad [5]$$

where $I_{EKT}$ is the vertical ionization energy of the system extracted from the ground-state interacting wavefunction via the extended Koopmans theorem (EKT) (45–48). For a Hartree–Fock wavefunction, Eq. **5** reduces to $\epsilon_{HOMO}^{KS} = \epsilon_{HOMO}^{HF}$ (42). As the accuracy of the wavefunction increases, $I_{EKT}$ tends (48, 49) to the exact first ionization energy $I$, which is the correct value of $-\epsilon_{HOMO}^{KS}$ in the exact Kohn–Sham scheme (50).

For atoms and molecules with a single-reference character, Kohn–Sham potentials derived from Hartree–Fock wavefunctions are practically indistinguishable from exact exchange-only (correlationless) OEPs (51, 52). In the absence of strong electron correlation, they are also very good approximations to the exact $v_{eff}^{KS}(\mathbf{r})$. We illustrate this general result in Figs. 1 and 2, which show typical atomic and molecular Kohn–Sham potentials and their classical turning points derived from Hartree–Fock, full-configuration interaction (FCI), and full-valence complete active space self-consistent field (CASSCF) wavefunctions, as well as from the Perdew–Burke–Ernzerhof (PBE) density-functional approximation (53) including correlation. In both Figs. 1 and 2, the turning points of the Kohn–Sham potentials obtained from Hartree–Fock and correlated wavefunctions are close to each other but are markedly different from the turning points of the PAEM. The PAEM-based radius of the sodium ion in the NaCl molecule is as much as 0.5 Å greater than the turning radius derived from the Kohn–Sham potential (Fig. 2). In fact, the entire $v_{eff}^{KS}(\mathbf{r})$-based molecular surfaces of NaCl derived from the Hartree–Fock and full-valence CASSCF wavefunctions are visually indistinguishable from each other and differ significantly from the PAEM surface (*SI Appendix*, Fig. S1). These observations suggest that it would be pointless to generate

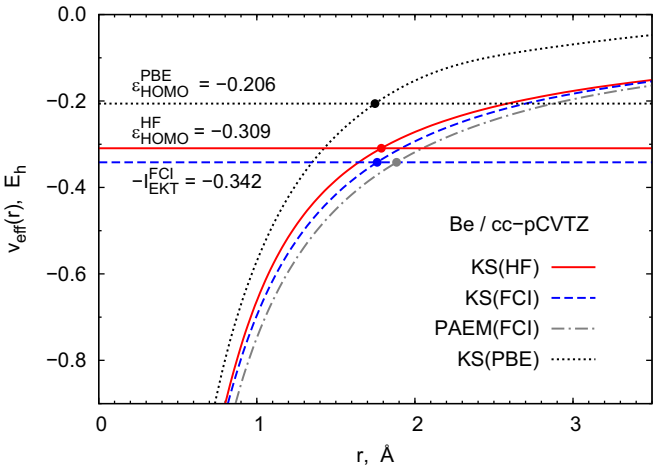


**Fig. 1.** Kohn–Sham effective potentials and the PAEM for the Be atom. Each potential is derived from the wavefunction or functional shown in parentheses. The circles mark the corresponding classical turning points.

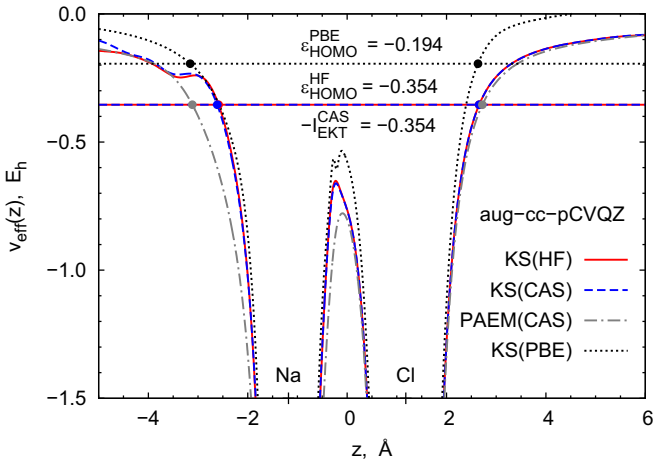


**Fig. 2.** Same as in Fig. 1 for the NaCl molecule at the experimental equilibrium geometry ($r_e = 2.3609$ Å). The correlated wavefunction is (8,8)CASSCF.

classical turning surfaces of $v^{KS}_{eff}(\mathbf{r})$ from correlated wavefunctions where a single Slater determinant would suffice. Therefore, all mRKS production runs here are at the Hartree–Fock level of theory.

Kohn–Sham effective potentials derived from standard density-functional approximations such as PBE are not negative enough and give too-high $\epsilon^{KS}_{HOMO}$ values. Each of these errors is large, but they counteract and, in some cases, cancel each other to produce a reasonably accurate classical turning surface (as in Fig. 1). In other cases, the cancellation of errors is incomplete and the PBE turning points are closer to those of the PAEM than to the turning points of accurate Kohn–Sham potentials (as in Fig. 2). Approximate density functionals are also known to give incorrect Kohn–Sham potentials for heteronuclear molecules with stretched bonds, a defect that is manifested in spurious fractional atomic charges (54–57) and is absent in the Hartree–Fock description (55, 56).

In this work, the nonrelativistic ground-state Hartree–Fock wavefunctions of neutral atoms and atomic cations were obtained using the universal Gaussian basis set (58) augmented with one set of polarization functions (UGBS1P); for anions, we used the same basis set with additional diffuse functions (UGBS1P+), as defined in the GAUSSIAN program (44). The polarization functions are needed only for nonspherical atoms. These basis sets are close to the basis-set limit. To construct molecular surfaces of molecules and protomolecules, we used correlation-consistent basis sets (59). All basis sets contained only pure $d$, $f$, etc., functions. The size of the basis set used in the mRKS method is not crucial: Smaller basis sets such as 6-31G* would have produced similar results for neutral atoms and cations.

All Hartree–Fock and mRKS calculations were spin unrestricted. Thus, for open-shell systems there were two distinct Kohn–Sham potentials, one for spin up and another for spin down; the one used in Eq. **1** corresponds to the spin channel of the highest occupied spin-orbital, which in all cases was the majority-spin channel. In the spin-unrestricted approach, Kohn–Sham potentials of atoms and ions with completely or half-filled electronic subshells (e.g., Li, Be, $B^+$, N,...) have spherically symmetric classical turning surfaces. For such atoms (ions), Eq. **1** was solved by interpolation on the numerical integration grid of the mRKS procedure. The turning radius of each nonspherical atom (ion) was determined as in ref. 9, that is, as the radius of a sphere whose volume is equal to the volume $V$ enclosed by the classical turning surface of the atom (ion); each $V$ was obtained by numerical integration. To achieve benchmark accuracy, all numerical integrations were performed using grids with 999 radial and 974 angular points per atom.

Note that transition-metal atoms and ions with incompletely filled $d$ subshells may have different occupations of differently shaped $d$ orbitals in the ground-state Hartree–Fock and Kohn–Sham wavefunctions. In such cases, a self-consistent Kohn–Sham potential corresponding to a given Hartree–Fock density could be challenging to converge and may not even exist.

## Results and Discussion

**Atomic and Ionic Radii.** Fig. 3 shows the Kohn–Sham potential-based atomic and ionic radii of the first 54 elements of the periodic table. The electron configurations, spin multiplicities, and HOMO energies of all these species (and some $A^{n+}$ ions with $n > 2$) are listed in *SI Appendix*, Table S1. A dash in Fig. 3 means either that the Hartree–Fock solution could not be found or that it gave $\epsilon^{HF}_{HOMO} > 0$. Most of the missing values are for transition-metal anions—systems that are challenging to describe reliably using finite basis sets.

The smallest neutral atom in Fig. 3 is He ($R = 0.62$ Å), and the largest is Rb ($R = 3.84$ Å). There are clear chemical trends. For a given element, all radii decrease as electrons are removed and more strongly so when this removal unveils an outer closed shell. For the neutral atoms, radii increase down a column of the periodic table, except for the Ni column, where there is a change of orbital configuration from Ni ($3d^8 4s^2$) to Pd ($3d^{10}$). The radii of the neutral atoms decrease across a row, except where a new subshell starts to fill, as in going from Be to B and from Ni to Cu. In the nonrelativistic limit of large atomic number, the radii of the neutral atoms are expected to approach column-dependent finite limits (60). The radii of singly and doubly positive ions follow the same trends as the radii of the corresponding isoelectronic neutral atoms.

The large-$r$ asymptote of the Kohn–Sham effective potential is $-(Z - N + 1)/r$. For a neutral atom, this is $-1/r$, but for a doubly negative ion it is $+1/r$. An electron in the doubly negative ion can escape quantum mechanically by tunneling through the corresponding potential barrier, but in classical physics it can still be bound inside a turning surface. In practice, doubly negative atomic ions such as $O^{2-}$ do not exist in the free state except as unstable scattering resonances, but are commonly assumed to be present in ionic solids (at least formally). To estimate the sizes of such anions, we extrapolated their radii using a third-order polynomial in electron number $N$ that is exact for $N = 1$, $Z - 1$, $Z$, and $Z + 1$ (*SI Appendix*). The resulting estimates are included in the Fig. 3 legend. Note that doubly negative ions were not considered in the work of Yang and coworkers (13–21).

Unlike the PAEM-based and density-based atomic radii, the classical turning radii of the Kohn–Sham potential never break the established periodic trends. In particular, the PAEM-based radii of neutral atoms always increase slightly (21) from group 15 to group 16 (e.g., $R = 1.34$ Å for N, $R = 1.38$ Å for O), whereas atomic radii derived from the Kohn–Sham potentials decrease (Fig. 3), in agreement with most other definitions (3, 5–8). The radii of Fig. 3 even rectify a defect of isodensity contour-based radii (9), which implausibly increase from group 1 (Na, K, Rb) to group 2 (Mg, Ca, Sr). Our definition also produces the expected inverse dependence of $R$ on $Z$ for one-electron atomic ions ($R = 2a_0/Z$), whereas a surface of constant density at $10^{-3}$ $e/a_0^3$ yields an unexpected result, $R = [\ln(10^3/\pi)/2Z + (3/2)\ln Z/Z]a_0$.

The correct behavior $R \sim 1/Z$ for a one-electron ion could alternatively be achieved by defining an isodensity surface outside of which we find a fixed number of electrons (e.g., 0.24 to

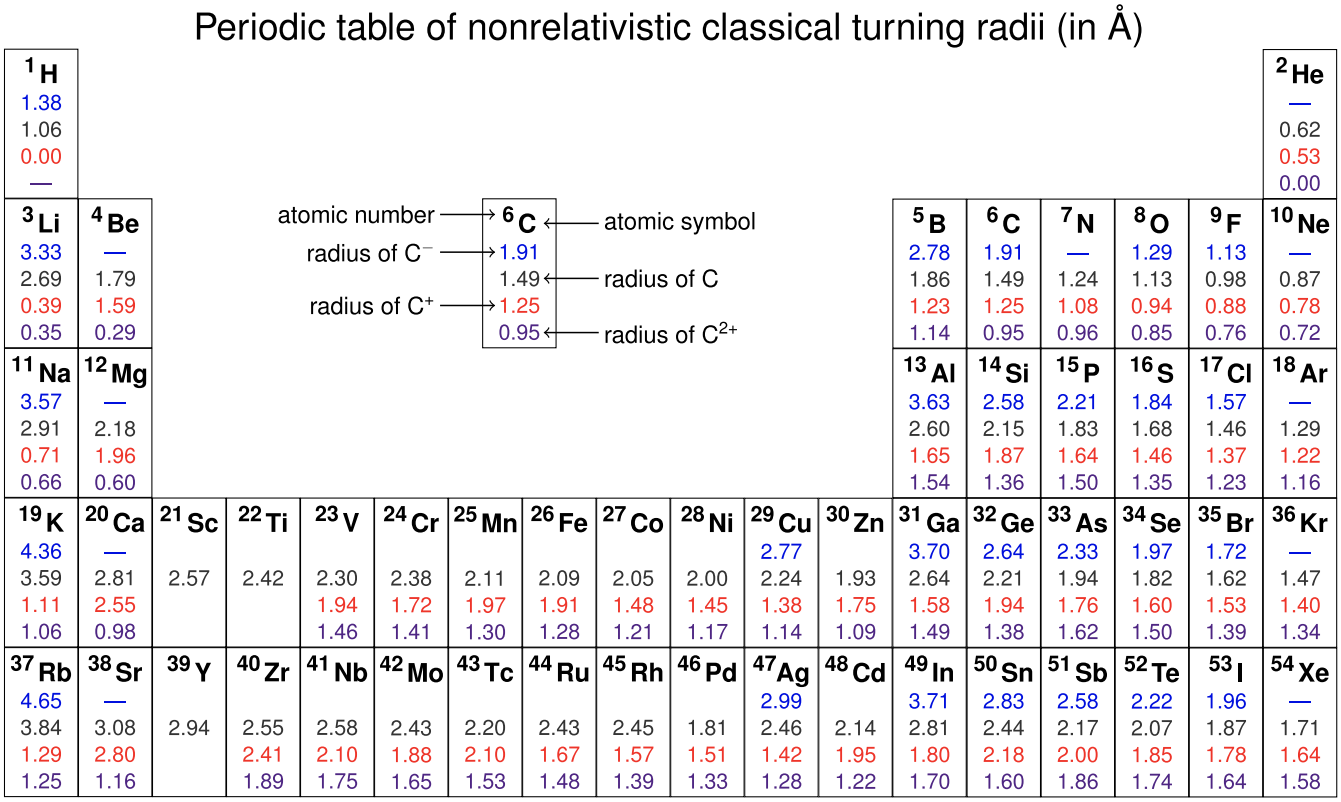


**Fig. 3.** Classical turning radii of the neutral atoms and ions of elements H through Xe. For each element A, the radii are shown for four different species: $A^-$ (in blue), A (in black), $A^+$ (in red), and $A^{2+}$ (in purple). All values are based on the Kohn–Sham potentials generated from spin-unrestricted HF/UGBS1P ground-state wavefunctions (HF/UGBS1P + for anions). The extrapolated radii of $O^{2-}$, $S^{2-}$, $Se^{2-}$, and $Te^{2-}$ are 1.41 Å, 1.92 Å, 2.05 Å, and 2.28 Å, respectively.

match the value from the classical turning surface of the one-electron ion). But that definition would fail for a large spherical uniform cluster, since the number of electrons outside the classical turning surface of its Kohn–Sham potential would grow like the surface area or square of its classical turning radius, leading to another unexpected logarithm in the expression for $R$. Another possibility is to define the radius of an electronic object as that of a sphere containing say 98% of the electron density (12), but that choice would predict very different radii for a uniform cluster and a similar cluster inside of which is embedded another cluster of much higher electron density. It is not easy to find a viable alternative to the classical turning surface of the Kohn–Sham potential.

Finally, it is instructive to compare our first-principles atomic radii to the crystallographic van der Waals radii recommended by Batsanov (5) for neutral atoms. For the 48 elements appearing both in our Fig. 3 and in table 9 of ref. 5, the mean atomic radii are 2.2 Å and 2.1 Å, respectively, and the mean absolute deviation of the one from the other is 0.3 Å. Standard van der Waals (6) and covalent radii of neutral molecules, designed to predict nearest-neighbor distances for nonbonded or covalently bonded neighbors, are respectively often much larger and always much smaller than our intrinsic radii.

**Bonding Types.** Classical turning surfaces of the Kohn–Sham effective potential can be used to identify the type of chemical bonding between two atoms, given the integer charge state of each. Consider the bond-specific ratio

$$\beta(\mathrm{AB}) = \frac{d_{\mathrm{AB}}}{R_{\mathrm{A}} + R_{\mathrm{B}}}, \qquad [6]$$

where $d_{\mathrm{AB}}$ is the internuclear separation of atoms (ions) A and B at the equilibrium molecular geometry, and $R_{\mathrm{A}}$ and $R_{\mathrm{B}}$ are their intrinsic classical turning radii. Table 1 lists $\beta$ values for diverse molecules representing three paradigmatic types of chemical bonds: covalent (nonpolar and polar), ionic, and van

**Table 1. Bond-type ratio ($\beta$) evaluated for representative gas-phase molecules using the equilibrium bond lengths ($d_{\mathrm{AB}}$) and the atomic and ionic radii from Fig. 3**

| Bond type | Molecule | AB | $d_{\mathrm{AB}}$, Å* | $\beta$(AB) |
|---|---|---|---|---|
| Covalent | $H_2$ | H–H | 0.74144 | 0.35 |
| | $N_2$ | N≡N | 1.0977 | 0.44 |
| | $F_2$ | F–F | 1.4119 | 0.72 |
| | $C_6H_6$ | C⋯C | 1.399 | 0.47 |
| | | C–H | 1.101 | 0.43 |
| | $H_2O$ | O–H | 0.9575 | 0.44 |
| | HF | H–F | 0.9169 | 0.45 |
| | HBr | H–Br | 1.4145 | 0.53 |
| Ionic | NaCl | $Na^+Cl^-$ | 2.3609 | 1.04 |
| | LiH | $Li^+H^-$ | 1.5949 | 0.90 |
| | LiF | $Li^+F^-$ | 1.5639 | 1.03 |
| Hydrogen | $(HF)_2$ | F⋯H | 1.820† | 0.89 |
| | $(H_2O)_2$ | O⋯H | 1.942† | 0.89 |
| | HCN⋯HF | N⋯H | 1.829† | 0.80 |
| Van der Waals | $Ne_2$ | Ne⋯Ne | 3.100‡ | 1.78 |
| | $Ar_2$ | Ar⋯Ar | 3.758‡ | 1.46 |

*Experimental values from ref. 61 unless noted otherwise.
†MP2(full)/aug-cc-pCVQZ value.
‡From ref. 62.

**Table 2. Bond-type ratio ($\beta$) evaluated for various cubic crystals using the experimental nearest-neighbor distances ($d$) from refs. 63 and 64 and the atomic and ionic radii from Fig. 3**

| Solid | $d$, Å* | $\beta$ |
|---|---|---|
| Ionic $M^+X^-$ (B1) | | |
| LiH | 2.05 | 1.16 |
| LiF | 2.01 | 1.32 |
| LiCl | 2.57 | 1.31 |
| LiBr | 2.75 | 1.30 |
| LiI | 3.01 | 1.28 |
| NaH | 2.44 | 1.17 |
| NaF | 2.31 | 1.26 |
| NaCl | 2.82 | 1.24 |
| NaBr | 2.99 | 1.23 |
| NaI | 3.24 | 1.21 |
| KH | 2.85 | 1.15 |
| KF | 2.67 | 1.19 |
| KCl | 3.15 | 1.17 |
| KBr | 3.30 | 1.17 |
| KI | 3.53 | 1.15 |
| RbH | 3.02 | 1.13 |
| RbF | 2.82 | 1.17 |
| RbCl | 3.29 | 1.15 |
| RbBr | 3.43 | 1.14 |
| RbI | 3.67 | 1.13 |
| AgF | 2.46 | 0.97 |
| AgCl | 2.78 | 0.93 |
| AgBr | 2.89 | 0.92 |
| Ionic $M^{2+}X^{2-}$ (B1) | | |
| MgO | 2.11 | 1.05 |
| MgS | 2.60 | 1.03 |
| MgSe | 2.73 | 1.03 |
| CaO | 2.41 | 1.01 |
| CaS | 2.85 | 0.98 |
| CaSe | 2.96 | 0.98 |
| CaTe | 3.18 | 0.98 |
| SrO | 2.56 | 0.99 |
| SrS | 3.01 | 0.98 |
| SrSe | 3.12 | 0.97 |
| SrTe | 3.33 | 0.97 |
| CdO | 2.35 | 0.89 |
| Covalent (diamond) | | |
| C | 1.54 | 0.52 |
| Si | 2.35 | 0.55 |
| Ge | 2.45 | 0.55 |
| $\alpha$-Si | 2.81 | 0.58 |
| van der Waals (fcc) | | |
| Ne | 3.13 | 1.80 |
| Ar | 3.75 | 1.45 |
| Kr | 3.99 | 1.36 |
| Xe | 4.33 | 1.27 |

*$d = a/2$ for rock-salt type, $d = a\sqrt{3}/4$ for diamond type, and $d = a/\sqrt{2}$ for fcc structures, where $a$ is the lattice constant.

der Waals. Examination of these data suggests that the following relationships tend to hold:

$$\beta \lesssim 0.7 \quad \text{(covalent bond)} \quad [7]$$

$$\beta \approx 0.9\text{–}1.3 \quad \text{(ionic bond)} \quad [8]$$

$$\beta \gtrsim 1.3 \quad \text{(van der Waals bond).} \quad [9]$$

Hydrogen bonds, as mixtures of these three bond types, can have $\beta$ values anywhere between 0.5 and 1, although quintessential cases fall into a narrower range of 0.7–0.9. Within each bond type, weak bonds tend to have larger $\beta$ values.

Eqs. **7** and **8** are analogous to the PAEM-based criteria suggested by Zhao et al. (21) as a means to distinguish between covalent and ionic bonds. Relation **7** is also implied in Batsanov's work (5), where pictures of strongly overlapping ($\beta \ll 1$) neutral-atom spheres of covalent solids appear prominently. The remainder of this section provides numerous other examples supporting the $\beta$-ratio approach to analyzing chemical bonding.

First, Eqs. **7–9** hold not only for gas-phase molecules, but also for solids (Table 2). For 35 rock-salt–type (B1) crystals that are commonly classified as ionic, the ratio $\beta$ ranges from 0.9 to 1.3 and averages to 1.1 with a mean absolute deviation of 0.1, in accord with Eq. **8**. For covalent solids in the diamond cubic crystal structure (C, Si, Ge, and gray Sn) we find $\beta = 0.52\text{–}0.58$, in agreement with Eq. **7**. Van der Waals-bonded face-centered cubic (fcc) crystals of noble-gas atoms have $\beta$ values ranging from 1.80 for Ne to 1.27 for Xe, in accord with Eq. **9**.

The $\beta$-ratio bond-type test assumes that one knows a priori the specific integer-charge states of the two atoms. If these states are unambiguous (as in $H_2$ and NaCl), then the value of $\beta$ clearly and objectively determines the bond type. In the absence of clear-cut charge-state information, possible $\beta$ values can be used to challenge misidentifications. Consider, for instance, the HF and HBr molecules. Assuming that their bonds are polar covalent, we have $\beta(\text{H–F}) = 0.45$ and $\beta(\text{H–Br}) = 0.53$, which are well within the typical range of $\beta$ values for covalent bonds. The assumption that the bonds are ionic would yield $\beta(H^+F^-) = 0.81$ and $\beta(H^+Br^-) = 0.82$. These values fall below the normal ionic range and thereby cast doubt on the assumption of ionicity.

Of course, the criteria of Eqs. **7–9** are imprecise, and there is a continuum between different bond types. The fact that the $\beta$ value for a particular bond does not fall within any paradigmatic type can be taken as an indication of a mixed-type bonding. The hydrogen bond by definition falls into this category. Another example is solids that are neither purely ionic nor covalent. Consider, for instance, crystalline CuCl ($d = 2.34$ Å), the bonding in which was discussed by Zhao et al. (21). Using the PAEM-based ionic radii from ref. 21, one has $\beta(Cu^+Cl^-) = 0.74$, whereas our Kohn–Sham potential-based ionic radii give $\beta(Cu^+Cl^-) = 0.79$ and $\beta(\text{CuCl}) = 0.63$. These values clearly indicate a mixed-type bonding that is more covalent than ionic. The zincblende structure of CuCl, taken by many semiconductors, also suggests a component of covalent bonding.

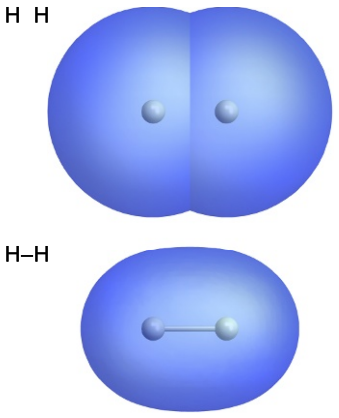


**Fig. 4.** Classical turning surfaces of the Kohn–Sham effective potential for the $H_2$ protomolecule and the $H_2$ molecule, both at the experimental equilibrium geometry of $H_2$ from Table 1. The Kohn–Sham potentials were derived from atomic and molecular HF/aug-cc-pVQZ wavefunctions. Here $\beta(\text{HH}) = 0.35$.

The $\beta$-ratio test also works for coordinate covalent (dative) bonds and for metal–ligand bonds in transition-metal complexes. For example, the $BF_3 \cdot NH_3$ donor–acceptor complex with $d_{BN} = 1.59$ Å has $\beta(BN) = 0.51$ and $\beta(B^-N^+) = 0.41$, indicating a covalent bond in either case. The complex $[FeCl_4]^{2-}$ with $d_{FeCl} = 2.30$ Å has $\beta(Fe^{2+}Cl^-) = 0.81$, which suggests an ionic bond with some covalent character. We find that metal–ligand bonds in transition-metal complexes tend to have $\beta$ values between 0.7 and 0.9, depending on the degree of their ionicity.

Apart from being a confirmation of what is already known, the value of $\beta$ can serve as a discovery tool in the quest for materials with targeted properties. For instance, in a high-throughput search for layered materials over many candidates of known structures, the inequality $\beta > 1$ could be used to identify the van der Waals bonds between layers that are easily exfoliated to make 2D materials.

**Covalent, Ionic, and van der Waals Molecules.** Classical turning surfaces of the Kohn–Sham effective potential can also be used to make revealing pictures of atoms, molecules, atomic clusters, molecular complexes, solid surfaces, and other microscopic chemical objects. We illustrate their usefulness in Figs. 4–7, which show the classical turning surfaces of the Kohn–Sham potentials for bonds of four different types: nonpolar covalent (H–H), polar covalent (H–Br), ionic ($Na^+Cl^-$), and van der Waals (Ne···Ne). Each of Figs. 4–7 also shows the classical turning surface of the corresponding protomolecule: the exterior part of the union of the spherical surfaces of the free atoms (ions) brought together at the experimental equilibrium molecular geometry.

Fig. 4 depicts how two strongly overlapping atomic spheres of the hydrogen protomolecule shrink and fuse seamlessly to form a covalently bonded $H_2$ molecule ($\beta \ll 1$). Similar results were found for protomolecular and molecular surfaces of HBr (Fig. 5), HF, and $N_2$ (*SI Appendix*).

In the ionically bonded NaCl molecule, the sodium and chlorine are more similar in size to the free $Na^+$ and $Cl^-$ ions than to the free neutral Na and Cl atoms (Fig. 6). This suggests that the protomolecule should be taken as a pair of $Na^+$ and $Cl^-$ ions. These ions overlap weakly if at all ($\beta \approx 1$) in the protomolecule and then fuse into the molecular NaCl surface with a distinct seam that preserves much of their identities (although the polarization of the $Cl^-$ ion is clearly visible). It is significant that this seam does not exist in the PAEM-based NaCl surface, which looks as smoothly fused as surfaces of covalent molecules (*SI Appendix*, Fig. S1). The seam is a distinctive but not universal visual feature of Kohn–Sham molecular surfaces for ionic bonds: Other ionic molecules such as LiF also have it, while molecules such as MgO do not (*SI Appendix*, Figs. S4 and S5).

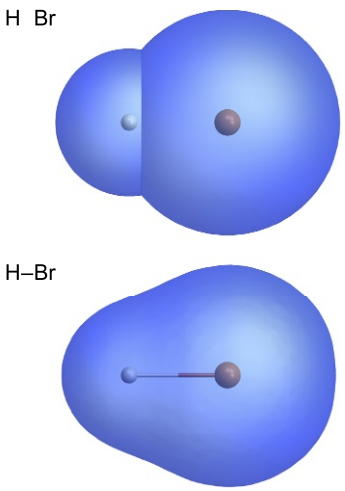


**Fig. 5.** Classical turning surfaces of the Kohn–Sham effective potential for the HBr protomolecule and the HBr molecule, both at the experimental equilibrium geometry of HBr from Table 1. The Kohn–Sham potentials were derived from atomic and molecular HF/aug-cc-pCVQZ wavefunctions. Here $\beta(HBr) = 0.53$, $\beta(H^+Br^-) = 0.82$.

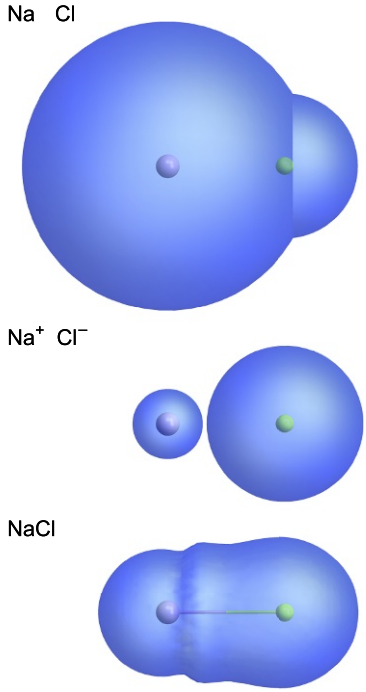


**Fig. 6.** Classical turning surfaces of the Kohn–Sham effective potential for the neutral-atom NaCl protomolecule, the ionic protomolecule ($Na^+Cl^-$), and the gas-phase NaCl molecule, all at the experimental equilibrium molecular geometry of NaCl from Table 1. The $Na^+$ ion is on the left. The Kohn–Sham potentials were derived from atomic and molecular HF/aug-cc-pCVQZ wavefunctions. Here $\beta(Na^+Cl^-) = 1.04$.

In the van der Waals-bonded neon dimer, the atomic spheres are disconnected and retain nearly all of their free-atom identities seen in the protodimer (Fig. 7), which suggests a noncovalent interaction ($\beta \gg 1$). Moreover, the two atomic spheres of the dimer remain disconnected and virtually unchanged even if the nuclei are forced as close as $d_{NeNe} = 0.6r_e$.

The water dimer, $(H_2O)_2$, is held together by an archetypal hydrogen bond. This bond shows up in the Kohn–Sham molecular surface of the dimer as a smooth narrow neck connecting the

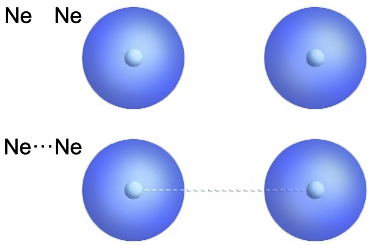


**Fig. 7.** Classical turning surfaces of the Kohn–Sham effective potential for the $Ne_2$ protodimer and the van der Waals-bonded $Ne_2$ molecule, both at the experimental equilibrium geometry of $Ne_2$ from Table 1. The Kohn–Sham potentials were derived from atomic and molecular HF/aug-cc-pCVQZ wavefunctions. Here $\beta(Ne \cdots Ne) = 1.78$.

CHEMISTRY

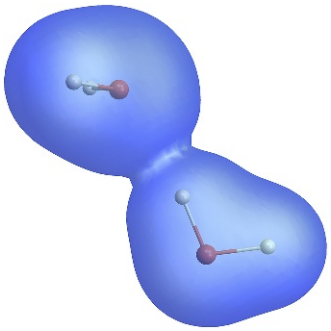

**Fig. 8.** Classical turning surface of the Kohn–Sham effective potential for the water dimer, $(H_2O)_2$, at the MP2(full)/aug-cc-pCVQZ geometry. The potential was derived from the HF/aug-cc-pCVQZ wavefunction. Here $\beta = 0.44$ for the four covalent O–H bonds and $\beta = 0.89$ for the hydrogen bond.

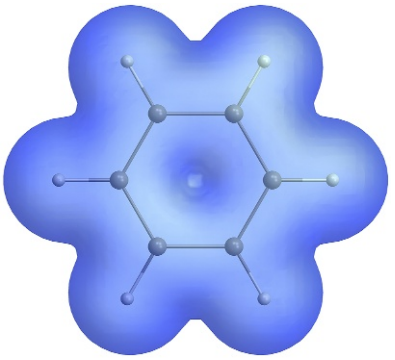

**Fig. 9.** Classical turning surface of the Kohn–Sham effective potential for the benzene ($C_6H_6$) molecule at the experimental equilibrium geometry from Table 1. The potential was derived from the HF/cc-pCVDZ wavefunction.

two water molecules (Fig. 8). The $\beta$ value for the hydrogen bond is 0.89, consistent with its hybrid nature.

The mRKS method can also be used with ease to generate classical turning surfaces of larger molecules such as benzene (Fig. 9). Note that the center of the benzene ring is a dimple and not a hole in the classical turning surface. More examples of Kohn–Sham classical turning surfaces of atoms, molecules, and their complexes are in *SI Appendix*.

## Concluding Remarks

Sharply defined surfaces of classical objects provide our first understanding of the world, while noninteracting quantum mechanical electrons moving in an effective potential provide our first understanding of atoms and the bonds between them. The classical turning surface of the Kohn–Sham effective potential defines the classical surface and thus the size and shape of a chemical species. It also identifies covalent, ionic, and van der Waals bonds in accord with chemical intuition. For covalently bonded molecules like $H_2$, HBr, and $C_6H_6$, this surface shows the smooth fusion of the constituent atoms. For ionic molecules like NaCl and LiF, there is a seam in the surface that preserves some of the identity of the separate ions. For van der Waals dimers like $Ne_2$, there are two separate surfaces, preserving nearly all of the identity of the constituents. For hydrogen-bonded water clusters, there is a neck in the surface between water molecules, arising from a weak overlap and merger of their individual molecular surfaces at the equilibrium hydrogen-bond length.

Our bond-type analysis using the $\beta$ ratio of Eq. **6** starts from a single first-principles radius for each atom (atomic ion) and a given bond length, deducing there from the nature of the bonding. The traditional empirical approaches (3, 4, 6–8) define atomic (ionic) radii as those $R$ values for which the ratio $\beta$ would be identically equal to 1.

In many cases, particularly for neutral atoms and covalent molecules, classical turning surfaces of the Kohn–Sham effective potential are similar in shape but not in size to classical turning surfaces of the PAEM. For ionic compounds, however, the Kohn–Sham potential and the PAEM produce qualitatively different results. The PAEM-based molecular surface does not capture the expected preservation of the chemical identity of the constituent ions, whereas the Kohn–Sham potential-based surface exhibits a distinct interatomic seam that preserves to some extent the identities of the negative and positive ions. Thus, the Kohn–Sham potential-based approach agrees with chemical intuition in all bonding situations.

The classical turning surface of the Kohn–Sham potential is also, via the Kohn–Sham one-electron Schrödinger equation, the surface on which the Laplacian of the Kohn–Sham HOMO vanishes,

$$\nabla^2 \phi^{\mathrm{KS}}_{\mathrm{HOMO}}(\mathbf{r}) = 0, \qquad [10]$$

a satisfyingly local condition. One might imagine using Eq. **10** with a Hartree–Fock or approximate Kohn–Sham HOMO to estimate the classical turning surface of an atom or molecule. [In practical calculations, this may require tricks for dealing with oscillations and divergences of the second derivatives of molecular orbitals expanded in Gaussian basis functions (65).]

A recent article, "Visualizing the microscopic world" (66), opens with the following statement: "The human being tends to dislike what he/she does not understand, and a perfect example concerns the microscopic world. In the quest for understanding it, visualization of its systems has always played a central role, particularly because the entities in question are invisible to the naked eye. In fact, images have been instrumental not only in understanding the molecular world but also in the dissemination of information in general. Usually, the best illustrations are based on general principles of good physical representation and graphic design, but the link between scientific concepts and visual representation is often difficult to achieve, in particular in the educational context." We believe that the classical turning surface of the Kohn–Sham effective potential can serve as such a link without compromises.

**ACKNOWLEDGMENTS.** This work was supported by the National Science Foundation under Grants DMR 1607868 (to J.P.P.) and CHE-1640584 (to J.T.) and by the Natural Sciences and Engineering Research Council of Canada under Grants RGPIN-2015-04814 and RGPAS 477791-2015 (to V.N.S.). J.T. also acknowledges support from Temple University (via J.P.P.).

1. Pauling L (1960) *The Nature of the Chemical Bond* (Cornell Univ Press, Ithaca, NY), 3rd Ed.
2. Arunan E, et al. (2011) Definition of the hydrogen bond (IUPAC recommendations 2011). *Pure Appl Chem* 83:1637–1641.
3. Bondi A (1964) Van der Waals volumes and radii. *J Phys Chem* 68:441–451.
4. Shannon RD (1976) Revised effective ionic radii and systematic studies of interatomic distances in halides and chalcogenides. *Acta Cryst A* 32:751–767.
5. Batsanov SS (2001) Van der Waals radii of elements. *Inorg Mater* 37:871–885.
6. Mantina M, Chamberlin AC, Valero R, Cramer CJ, Truhlar DG (2009) Consistent van der Waals radii for the whole main group. *J Phys Chem A* 113:5806–5812.
7. Hu SZ, Zhou ZH, Xie ZX, Robertson BE (2014) A comparative study of crystallographic van der Waals radii. *Z Krystallogr Cryst Mater* 229:517–523.
8. Slater JC (1964) Atomic radii in crystals. *J Chem Phys* 41:3199–3204.
9. Rahm M, Hoffmann R, Ashcroft NW (2016) Atomic and ionic radii of elements 1–96. *Chem Eur J* 22:14625–14632.
10. Boyd RJ (1977) The relative sizes of atoms. *J Phys A: At Mol Phys* 10:2283–2291.
11. Politzer P, Parr RG, Murphy DR (1983) Relationships between atomic chemical potentials, electrostatic potentials, and covalent radii. *J Chem Phys* 79:3859–3861.
12. Kammeyer CW, Whitman DR (1972) Quantum mechanical calculation of molecular radii. I. Hydrides of elements of periodic groups IV through VII. *J Chem Phys* 56: 4419–4421.

13. Yang ZZ, Davidson ER (1997) Evaluation of a characteristic atomic radius by an *ab initio* method. *Int J Quantum Chem* 62:47–53.
14. Yang ZZ, Li GH, Zhao DX, He HB, Sun R (1998) Theoretical study on characteristic ionic radii. *Chin Sci Bull* 43:1452–1455.
15. Yang ZZ, Zhao DX (1998) A characteristic molecular contour evaluated by a theoretical method. *Chem Phys Lett* 292:387–393.
16. Zhao DX, Yang ZZ (1999) Theory on the molecular characteristic contour(I)—A new approach to defining molecular characteristic contour. *Sci China Ser B* 42:391–399.
17. Zhang MB, Zhao DX, Yang ZZ (2005) The characteristic boundary radii of atoms. *J Theor Comput Chem* 4:281–288.
18. Zhao DX, Yang ZZ (2008) Molecular face—A novel molecular model showing both molecular spatial contour and frontier electron density. *J Theor Comput Chem* 7:303–315.
19. Gong LD, Yang ZZ (2010) Investigation of the molecular surface area and volume: Defined and calculated by the molecular face theory. *J Comput Chem* 31:2098–2108.
20. Zhao DX, Yang ZZ (2014) Investigation of the distinction between van der Waals interaction and chemical bonding based on the PAEM-MO diagram. *J Comput Chem* 35:965–977.
21. Zhao DX, et al. (2018) An intrinsic criterion of defining ionic or covalent character of AB-type crystals based on the turning boundary radii calculated by an *ab initio* method. *Mol Phys* 116:969–977.
22. Parr RG, Yang W (1989) *Density-Functional Theory of Atoms and Molecules* (Oxford Univ Press, New York).
23. Slater JC (1951) A simplification of the Hartree–Fock method. *Phys Rev* 81:385–390.
24. Ou-Yang H, Levy M (1990) Theorem for exact local exchange potential. *Phys Rev Lett* 65:1036–1039.
25. Gaiduk AP, Staroverov VN (2009) How to tell when a model Kohn–Sham potential is not a functional derivative. *J Chem Phys* 131:044107.
26. Perdew JP, Parr RG, Levy M, Balduz JL Jr (1982) Density-functional theory for fractional particle number: Derivative discontinuities of the energy. *Phys Rev Lett* 49:1691–1694.
27. Gritsenko OV, Baerends EJ (1996) Effect of molecular dissociation on the exchange-correlation Kohn–Sham potential. *Phys Rev A* 54:1957–1972.
28. Kohut SV, Polgar AM, Staroverov VN (2016) Origin of the step structure of molecular exchange-correlation potentials. *Phys Chem Chem Phys* 18:20938–20944.
29. Ryabinkin IG, Ospadov E, Staroverov VN (2017) Exact exchange-correlation potentials of singlet two-electron systems. *J Chem Phys* 147:164117.
30. Kohn W, Sham LJ (1965) Self-consistent equations including exchange and correlation effects. *Phys Rev* 140:A1133–A1138.
31. Jones RO (2015) Density functional theory: Its origins, rise to prominence, and future. *Rev Mod Phys* 87:897–923.
32. Levy M (1982) Electron densities in search of Hamiltonians. *Phys Rev A* 26:1200–1208.
33. Lieb EH (1983) Density functionals for Coulomb systems. *Int J Quantum Chem* 24: 243–277.
34. Baerends EJ, Gritsenko OV (1997) A quantum chemical view of density functional theory. *J Phys Chem A* 101:5383–5403.
35. Cuevas-Saavedra R, Staroverov VN (2016) Exact expressions for the Kohn–Sham exchange-correlation potential in terms of wave-function-based quantities. *Mol Phys* 114:1050–1058.
36. Staroverov VN (April 19, 2018) Contracted Schrödinger equation and Kohn–Sham effective potentials. *Mol Phys*, 10.1080/00268976.2018.1463470.
37. Filippi C, Gonze X, Umrigar CJ (1996) *Recent Developments and Applications of Modern Density Functional Theory*, ed Seminario JM (Elsevier, Amsterdam), pp 295–326.
38. Wu Q, Yang W (2003) A direct optimization method for calculating density functionals and exchange–correlation potentials from electron densities. *J Chem Phys* 118:2498–2509.
39. Engel E, Dreizler RM (1999) From explicit to implicit density functionals. *J Comput Chem* 20:31–50.
40. Staroverov VN, Scuseria GE, Davidson ER (2006) Optimized effective potentials yielding Hartree–Fock energies and densities. *J Chem Phys* 124:141103.
41. Ryabinkin IG, Kohut SV, Staroverov VN (2015) Reduction of electronic wavefunctions to Kohn–Sham effective potentials. *Phys Rev Lett* 115:083001.
42. Cuevas-Saavedra R, Ayers PW, Staroverov VN (2015) Kohn–Sham exchange-correlation potentials from second-order reduced density matrices. *J Chem Phys* 143:244116.
43. Ospadov E, Ryabinkin IG, Staroverov VN (2017) Improved method for generating exchange-correlation potentials from electronic wave functions. *J Chem Phys* 146:084103.
44. Frisch MJ, et al. (2016) *Gaussian Development Version, Revision I.13* (Gaussian, Inc., Wallingford, CT).
45. Day OW, Smith DW, Garrod C (1974) A generalization of the Hartree–Fock one-particle potential. *Int J Quantum Chem Symp* 8:501–509.
46. Smith DW, Day OW (1975) Extension of Koopmans' theorem. I. Derivation. *J Chem Phys* 62:113–114.
47. Day OW, Smith DW, Morrison RC (1975) Extension of Koopmans' theorem. II. Accurate ionization energies from correlated wavefunctions for closed-shell atoms. *J Chem Phys* 62:115–119.
48. Morrell MM, Parr RG, Levy M (1975) Calculation of ionization potentials from density matrices and natural functions, and the long-range behavior of natural orbitals and electron density. *J Chem Phys* 62:549–554.
49. Ernzerhof M (2009) Validity of the extended Koopmans' theorem. *J Chem Theory Comput* 5:793–797.
50. Levy M, Perdew JP, Sahni V (1984) Exact differential equation for the density and ionization energy of a many-particle system. *Phys Rev A* 30:2745–2748.
51. Ryabinkin IG, Kananenka AA, Staroverov VN (2013) Accurate and efficient approximation to the optimized effective potential for exchange. *Phys Rev Lett* 111:013001.
52. Kohut SV, Ryabinkin IG, Staroverov VN (2014) Hierarchy of model Kohn–Sham potentials for orbital-dependent functionals: A practical alternative to the optimized effective potential method. *J Chem Phys* 140:18A535.
53. Perdew JP, Burke K, Ernzerhof M (1996) Generalized gradient approximation made simple. *Phys Rev Lett* 77:3865–3868.
54. Perdew JP, Zunger A (1981) Self-interaction correction to density-functional approximations for many-electron systems. *Phys Rev B* 23:5048–5079.
55. Ruzsinszky A, Perdew JP, Csonka GI, Vydrov OA, Scuseria GE (2006) Spurious fractional charge on dissociated atoms: Pervasive and resilient self-interaction error of common density functionals. *J Chem Phys* 125:194112.
56. Kim MC, Sim E, Burke K (2013) Understanding and reducing errors in density functional calculations. *Phys Rev Lett* 111:073003.
57. Komsa DN, Staroverov VN (2016) Elimination of spurious fractional charges in dissociating molecules by correcting the shape of approximate Kohn–Sham potentials. *J Chem Theory Comput* 12:5361–5366.
58. de Castro EVR, Jorge FE (1998) Accurate universal Gaussian basis set for all atoms of the periodic table. *J Chem Phys* 108:5225–5229.
59. Schuchardt KL, et al. (2007) Basis set exchange: A community database for computational sciences. *J Chem Inf Model* 47:1045–1052.
60. Constantin LA, Snyder JC, Perdew JP, Burke K (2011) Ionization potentials in the limit of large atomic number. *J Chem Phys* 133:241103.
61. Rumble JR, ed (2018) *CRC Handbook of Chemistry and Physics* (CRC Press, Boca Raton, FL), 99th Ed.
62. Johnson RD III (2018) NIST Computational Chemistry Comparison and Benchmark Database, NIST Standard Reference Database Number 101, Release 19. Available at, cccbdb.nist.gov. Accessed July 9, 2018.
63. Donnay JDH, Ondik HM, eds (1973) *Crystal Data Determinative Tables. Inorganic Compounds* (US Department of Commerce, National Bureau of Standards, Washington, DC), 3rd Ed, Vol 2.
64. Ashcroft NW, Mermin ND (1976) *Solid State Physics* (Holt, Rinehart and Winston, New York).
65. Gaiduk AP, Ryabinkin IG, Staroverov VN (2013) Removal of basis-set artifacts in Kohn–Sham potentials recovered from electron densities. *J Chem Theory Comput* 9:3959–3964.
66. Cerqueira NMFSA, Fernandes PA, Ramos MJ (2018) Visualizing the microscopic world. *Interdiscip Sci Comput Life Sci* 10:105–110.